IEEE Photonics Journal
An IEEE Photonics Society Publication

Open Access

Broadband Image-Reject Mixing Based on a Polarization-Modulated Dual-Channel Photonic Microwave Phase Shifter

Volume 12, Number 2, April 2020

Yamei Zhang, *Member, IEEE*
Zhaoyu Li
Wenjuan Chen
Ce Liu
Kunlin Shao
Dan Zhu, *Member, IEEE*
Shilong Pan, *Senior Member, IEEE*

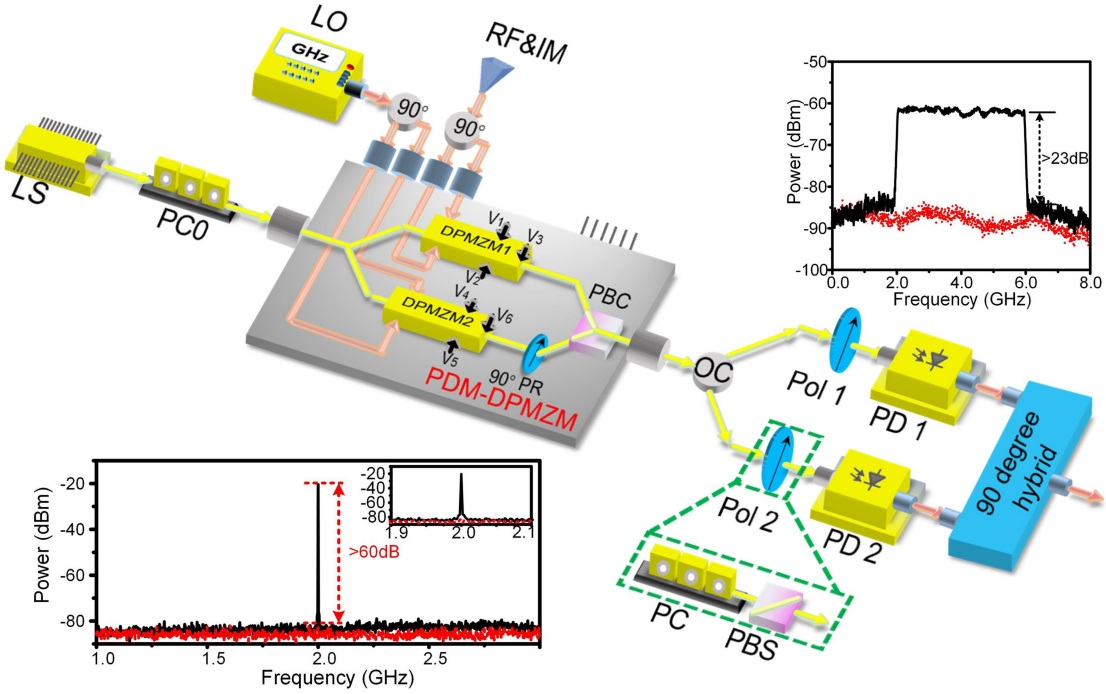

DOI: 10.1109/JPHOT.2020.2978148

Broadband Image-Reject Mixing Based on a Polarization-Modulated Dual-Channel Photonic Microwave Phase Shifter

Yamei Zhang, *Member, IEEE*, Zhaoyu Li, Wenjuan Chen, Ce Liu, Kunlin Shao, Dan Zhu, *Member, IEEE*, and Shilong Pan, *Senior Member, IEEE*

Key Laboratory of Radar Imaging and Microwave Photonics, Ministry of Education, Nanjing University of Aeronautics and Astronautics, Nanjing 210016, China

DOI:10.1109/JPHOT.2020.2978148
This work is licensed under a Creative Commons Attribution 4.0 License. For more information, see http://creativecommons.org/licenses/by/4.0/

Manuscript received January 26, 2020; revised February 25, 2020; accepted February 28, 2020. Date of publication March 3, 2020; date of current version March 18, 2020. This work was supported in part by National Natural Science Foundation of China under Grants 61901215 and 61527820, in part by National Key R&D Program of China under Grant 2018YFB2201803, and in part by the Fundamental Research Funds for the Central Universities. Corresponding author: Shilong Pan (e-mail: pans@nuaa.edu.cn).

Abstract: Broadband image-reject mixing using a dual-channel polarization-modulated photonic microwave phase shifter is proposed and experimentally demonstrated. The polarization-modulated photonic microwave phase shifter is realized by an orthogonal circularly-polarized wavelength generator, an optical coupler, two polarizers, and two photodetectors (PDs). When a local oscillator (LO) signal, a radio-frequency (RF) signal, and an image interference are supplied to the polarization-modulated phase shifter, opposite phase shifts would be introduced to the RF- and image-induced intermediate frequency (IF) signals. By carefully adjusting the polarizers to make the two channels of the phase shifter quadrature, a phase difference of −90 degree is introduced to the RF-induced IF signals in the two channels, while 90-degree phase difference between the image-induced IF signals is produced. With an electrical 90 degree hybrid to combine the two channels, the two RF-induced IF signals will be in phase while those from the image are out of phase. As a result, the image in the downconverted signal is cancelled. An experiment is carried out. An image-reject mixer (IRM) with an image rejection ratio of ∼60 dB for a single-frequency signal and 23 dB for a 4-GHz linear frequency-modulated signal is obtained.

Index Terms: Image-reject mixer, phase shifter, microwave photonics.

1. Introduction

Photonic microwave mixers are considered as an essential part in RF transceivers for radio over fiber systems, radar frontends and satellite payloads to convert the received high-frequency signals to a specific frequency band thanks to the advantages brought by the photonic technologies with respect to high frequency, large operational bandwidth, low transmission loss, and immunity to electromagnetic interference [1]–[5]. Generally, the photonic microwave mixer can be realized with two electro-optic modulators or an integrated electro-optic modulator with two radio-frequency (RF) input ports [6]–[10], e.g., two cascaded Mach-Zehnder modulators (MZMs) [6], cascaded MZM and electro-absorption modulator (EAM) [7], a dual-drive MZM, and a dual-parallel MZM (DPMZM) [8]–[10]. Applying a local oscillator (LO) signal and an RF signal to the two RF ports of the modulators, an intermediate frequency (IF) signal with its frequency equal to the difference of the two input

signals can be generated ($\omega_{\mathrm{IF}} = \omega_{\mathrm{RF}} - \omega_{\mathrm{LO}}$, where ω_{IF}, ω_{RF} and ω_{LO} represent the angular frequencies of the IF, RF and LO signals, respectively. For convenience, we assume that $\omega_{\mathrm{LO}} < \omega_{\mathrm{RF}}$). With the fast development of the RF technology, the spectrum environment for an RF system becomes more and more intricate. The inputs of the mixer may contain large image components centered at $\omega_{\mathrm{IM}} = \omega_{\mathrm{LO}} - \omega_{\mathrm{IF}}$, where ω_{IM} is the angular frequency of the image, producing a signal with a frequency of ω_{IF} at the output, which would superimpose with the desired signal in the spectral domain. As a result, an image-reject mixer (IRM) that has a large image suppression ratio is highly desired.

Generally, there are two methods to suppress the images in the photonic microwave mixer. One is using electrical filters [11], [12] to directly remove the images in the received signals in the electrical domain, or using optical filters [13], [15] to remove the optical sidebands introduced by the images. This method has a simple structure but suffers from limited operation bandwidth and poor frequency tunability, and it would not be effective when the frequency of the IF signal is very small.

The other approach for image rejection is implemented based on phase cancellation [16]–[26]. The key is to generate two out-of-phase image-induced IF signals before coherent combination. To do so, the well-known Hartley architecture is proposed [2], in which two parallel single-ended mixers and a pair of quadrature LO signals are required. When an RF signal and its image are sent to the two mixers, two pairs of oppositely quadrature IF signals can be generated, i.e., the phase difference between the two RF-induced IF signals is -90 degree while that between the two image-induced IF signals is 90 degree. With an electrical 90 degree hybrid to combine the two outputs of the parallel mixers, the phase differences change to be 0 and 180 degree, i.e., the RF-induced IF signals are in phase while the image-induced IF signals are out of phase. As a result, the image can be suppressed. Based on this scheme, an optical 90 degree hybrid is employed to introduce the quadrature LO signals in an IRM structure [16]–[19]. However, the unideal 90 degree phase shift of the optical 90 degree hybrid would lead to a relatively small image rejection ratio. To solve this problem, broadband tunable photonic microwave phase shifters are used to introduce the precise phase shift [22]–[26]. For example, in [23], a photonic microwave phase shifter based on a dual-drive Mach-Zehnder modulator (DMZM) incorporated with an optical bandpass filter (OBPF) is employed to realize an IRM. However, the employment of optical filter would confine the operation bandwidth and the tunability of the IRM [22]–[25]. In [26], cascaded modulators are required to implement the phase shifting function, which would increase the cost and the complexity of the IRM. In addition, in most of the reported IRMs, the broadband image suppression capability is not evaluated.

In this paper, a broadband and filterless photonic microwave IRM is proposed and experimentally demonstrated based on a dual-channel polarization-modulated photonic microwave phase shifter. The dual-channel phase shifter is realized by an orthogonal circularly-polarized wavelength generator, an optical coupler (OC), two polarizers and two photodetectors (PDs) [27], [28]. The phase shifts of the two channels can be independently and continuously tuned by the polarizer in each channel, and opposite phase shifts could be introduced to the RF- and image-induced IF signals. By carefully adjusting the polarizers in the two channels, two RF-induced IF signals with a phase difference of -90 degree and two image-induced IF signals with a phase difference of 90 degree can be obtained. With an electrical 90-degree hybrid to combine the two channels, the interference introduced by the image can be rejected. Since no optical filter or electrical filter is adopted, the IRM can work over a large wavelength range and has a good frequency tunability, which allows the system to be used in a wavelength-division multiplexed (WDM) system. In addition, thanks to the good scalability and phase tunability of the polarization-based photonic microwave phase shifter, the IRM can be easily scaled into multiple channels to realize multi-channel IRMs with independent phase shifts by sharing the same laser source and the same modulator, and the phase variations introduced by the electrical 90-degree hybrids can be properly compensated.

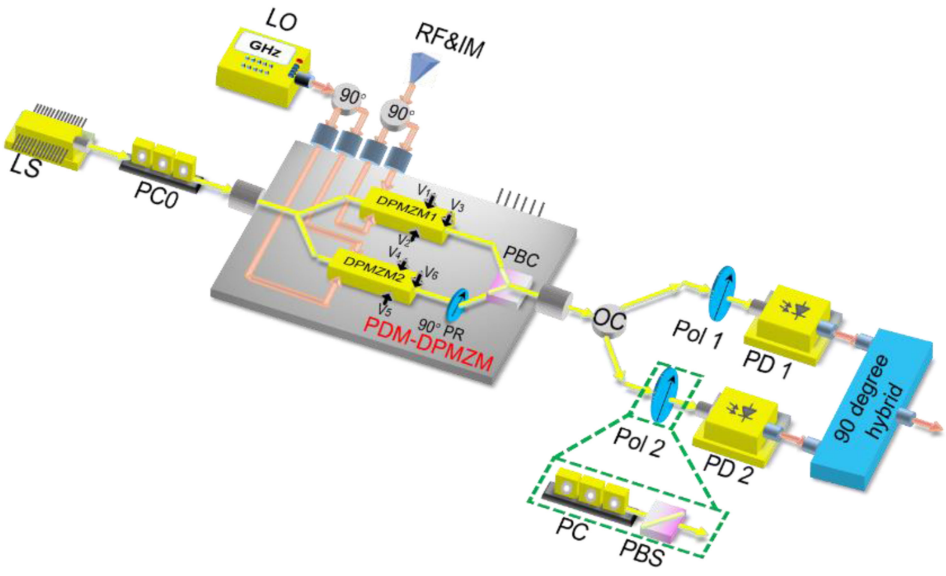

Fig. 1. Schematic diagram of the polarization-modulated IRM. LS: laser source; PC: polarization controller; PDM-DPMZM: polarization division multiplexing dual-parallel Mach-Zehnder modulator; PBC: polarization beam combiner; OC: optical coupler; Pol: polarizer; PD: photodetector; LO: local oscillator; IM: image; PR: polarization rotator; PBS: polarization beam splitter.

2. Experimental Setup

Fig. 1 shows the schematic diagram of the proposed IRM, which consists of a two-channel photonic microwave phase shifter and an electrical 90 degree hybrid. The photonic microwave phase shifter is realized by a laser source (LS), a polarization division multiplexing dual-parallel Mach-Zehnder modulator (PDM-DPMZM), an optical coupler, two polarizers, two PDs and two electrical 90 degree hybrids. The PDM-DPMZM together with the two 90 degree hybrids realizes an orthogonally-polarized wavelength generator [28]. When a lightwave and two pairs of quadrature RF signals with expressions of $\exp(j\omega_c t)$, $V_{\rm LO}\cos(\omega_{\rm LO}t+\phi_{\rm LO})$ and $V_{\rm LO}\cos(\omega_{\rm LO}t+\phi_{\rm LO}+\pi/2)$, and $V_{\rm RF}\cos(\omega_{\rm RF}t+\phi_{\rm RF})$ and $V_{\rm RF}\cos(\omega_{\rm RF}t+\phi_{\rm RF}+\pi/2)$ are applied to the PDM-DPMZM, where $V_{\rm RF}$ and $V_{\rm LO}$ are the amplitudes of the RF and LO signals, and $\phi_{\rm RF}$ and $\phi_{\rm LO}$ are the initial phases of the RF and LO signal, orthogonally-polarized carrier-suppressed single sideband (CS-SSB) modulations can be realized by each sub-DPMZM via adjusting the DC biases [28],

$$\begin{cases} E_x = -2J_{\pm1}\left(\beta_{\rm LO}\right)\exp\left[j\left(\omega_c t \pm \omega_{\rm LO}t \pm \phi_{\rm LO} \pm \pi/2\right)\right] \\ E_y = -2J_{\pm1}\left(\beta_{\rm RF}\right)\exp\left[j\left(\omega_c t \pm \omega_{\rm RF}t \pm \phi_{\rm RF} \pm \pi/2\right)\right] \end{cases}, \tag{1}$$

where x and y are on behalf of the two orthogonal axes of the PDM-DPMZM, $\beta_i = \pi V_i/V_\pi$ (i = RF, LO) are the modulation indices, V_π is the half-wave voltage of the PDM-DPMZM. In (1), small-signal modulation is assumed so that sidebands with orders larger than 2 are neglected. The signal in (1) is then split into two paths, and each path is followed by a polarizer and a PD to realize a photonic microwave phase shifter [27]. The expressions of the output current of the two phase shifters are,

$$I_{\rm IF-1}(t) \propto 2J_{\pm1}\left(\beta_{\rm LO}\right)J_{\pm1}\left(\beta_{\rm RF}\right)\cos\left(\omega_{\rm LO}t-\omega_{\rm RF}t+\phi_{\rm LO}-\phi_{\rm RF}-2\alpha_1\right), \tag{2}$$

and

$$I_{\rm IF-2}(t) \propto 2J_{\pm1}\left(\beta_{\rm LO}\right)J_{\pm1}\left(\beta_{\rm RF}\right)\cos\left(\omega_{\rm LO}t-\omega_{\rm RF}t+\phi_{\rm LO}-\phi_{\rm RF}-2\alpha_2\right), \tag{3}$$

where α_1 and α_2 are the angles between the polarization directions of the polarizers and one principal axis of the PDM-DPMZM. By simply controlling the angles between the polarizer and

one principal axis of the PDM-DPMZM, the phases of the two generated IF signals can be independently and continuously tuned while the magnitudes remain unchanged. Therefore, a two-channel photonic microwave phase shifter is realized.

If an image signal is applied to the PDM-DPMZM in conjunction with the useful RF signal, the output of the PDM-DPMZM can be rewritten as,

$$\begin{cases} E_x = -2J_{\pm1}\left(\beta_{\mathrm{RF}}\right)\exp\left[j\left(\omega_c t \pm \omega_{\mathrm{RF}} t \pm \phi_{\mathrm{RF}} \pm \pi/2\right)\right] - 2J_{\pm1}\left(\beta_{\mathrm{IM}}\right)\exp\left[j\left(\omega_c t \pm \omega_{\mathrm{IM}} t \pm \phi_{\mathrm{IM}} \pm \pi/2\right)\right] \\ E_y = -2J_{\pm1}\left(\beta_{\mathrm{LO}}\right)\exp\left[j\left(\omega_c t \pm \omega_{\mathrm{LO}} t \pm \phi_{\mathrm{LO}} \pm \pi/2\right)\right], \end{cases} \tag{4}$$

where β_{IM} represents the modulation index induced by the image signal. Then the outputs of the two PDs change to be,

$$\begin{aligned} I_{\mathrm{IF}-1}(t) &\propto 2J_{\pm1}\left(\beta_{\mathrm{LO}}\right)J_{\pm1}\left(\beta_{\mathrm{RF}}\right)\cos\left(\omega_{\mathrm{LO}} t - \omega_{\mathrm{RF}} t + \phi_{\mathrm{LO}} - \phi_{\mathrm{RF}} - 2\alpha_1\right) \\ &\quad + 2J_{\pm1}\left(\beta_{\mathrm{LO}}\right)J_{\pm1}\left(\beta_{\mathrm{IM}}\right)\cos\left(\omega_{\mathrm{IM}} t - \omega_{\mathrm{LO}} t + \phi_{\mathrm{IM}} - \phi_{\mathrm{LO}} + 2\alpha_1\right), \end{aligned} \tag{5}$$

$$\begin{aligned} I_{\mathrm{IF}-2}(t) &\propto 2J_{\pm1}\left(\beta_{\mathrm{LO}}\right)J_{\pm1}\left(\beta_{\mathrm{RF}}\right)\cos\left(\omega_{\mathrm{LO}} t - \omega_{\mathrm{RF}} t + \phi_{\mathrm{LO}} - \phi_{\mathrm{RF}} - 2\alpha_2\right) \\ &\quad + 2J_{\pm1}\left(\beta_{\mathrm{LO}}\right)J_{\pm1}\left(\beta_{\mathrm{IM}}\right)\cos\left(\omega_{\mathrm{IM}} t - \omega_{\mathrm{LO}} t + \phi_{\mathrm{IM}} - \phi_{\mathrm{LO}} + 2\alpha_2\right), \end{aligned} \tag{6}$$

By adjusting the polarizers to let α_1 to be 0 and α_2 to be 45 degree, the phase differences between the two RF-induced IF signals and the two image-induced IF signals are -90 degree and 90 degree, respectively. With an electrical low-frequency 90 degree hybrid to combine the two phase-shifted channels (introducing a 90 degree phase shift to $I_{\mathrm{IF}\text{-}2}$), the two RF-induced IF signals are in phase while the two image-induced IF signals are out of phase. Therefore, the output of the low-frequency 90 degree hybrid can be expressed as,

$$I_{\mathrm{IF}}(t) \propto 4J_{\pm1}\left(\beta_{\mathrm{LO}}\right)J_{\pm1}\left(\beta_{\mathrm{RF}}\right)\cos\left(\omega_{\mathrm{LO}} t - \omega_{\mathrm{RF}} t + \phi_{\mathrm{LO}} - \phi_{\mathrm{RF}}\right), \tag{7}$$

As a result, the interference introduced by the images are successfully suppressed. Since the polarization-modulated phase shifter has a large operation bandwidth and can be continuously tuned over 360-degree range, the IRM could be working over a large bandwidth too.

If the phase introduced by the low-frequency 90 degree hybrid is not 90 degree, e.g., $\varphi_{\mathrm{hybrid}} =$ 85 degree, the image signal can also be suppressed by controlling α_1 to be 0 and α_2 to be 47.5 degree, and the output signal can be expressed as,

$$I_{\mathrm{IF}}(t) \propto 2mJ_{\pm1}\left(\beta_{\mathrm{LO}}\right)J_{\pm1}\left(\beta_{\mathrm{RF}}\right)\cos\left(\omega_{\mathrm{LO}} t - \omega_{\mathrm{RF}} t + \phi_{\mathrm{LO}} - \phi_{\mathrm{RF}} + d\phi\right) \tag{8}$$

where,

$$\begin{aligned} m &= \sqrt{2 + 2\cos\left(2\alpha_2 - \varphi_{\mathrm{hybrid}}\right)} \\ d\phi &= \arctan\frac{\sin\left(2\alpha_2 - \varphi_{\mathrm{hybrid}}\right)}{1 + \cos\left(2\alpha_2 - \varphi_{\mathrm{hybrid}}\right)} \end{aligned} \tag{9}$$

As a result, the image can also be rejected. That is to say, the phase variation introduced by the electrical 90 degree hybrids can be properly compensated, but the power of the output IF signal would be decreased.

3. Experimental Result and Discussion

To demonstrate the feasibility of the proposed IRM in Fig. 1, an experiment is carried out. A lightwave with a wavelength of 1550.12 nm and a power of 14 dBm is generated by an LS and sent to a PDM-DPMZM (Fujitsu FTM 7977HQA) via a PC. The bandwidth and half-wave voltage of the PDM-DPMZM are 23 GHz and 3.5 V, respectively. The modulator is driven by a pair of quadrature RF signals and a pair of quadrature LO signals, which are obtained by splitting two outputs of a four-port vector network analyzer (VNA, R&S ZVA67) via two electrical 90 degree hybrids (1.7−36 GHz). By carefully controlling the output voltage of the DC suppliers that connected to the PDM-DPMZM, orthogonal-polarized CS-SSB modulated signals can be generated by the

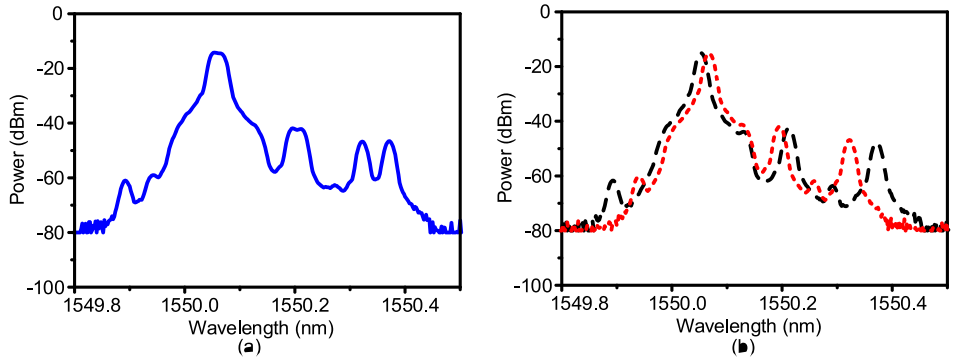

Fig. 2. (a) The optical spectra output from the PDM-DPMZM and (b) the outputs of the PBS.

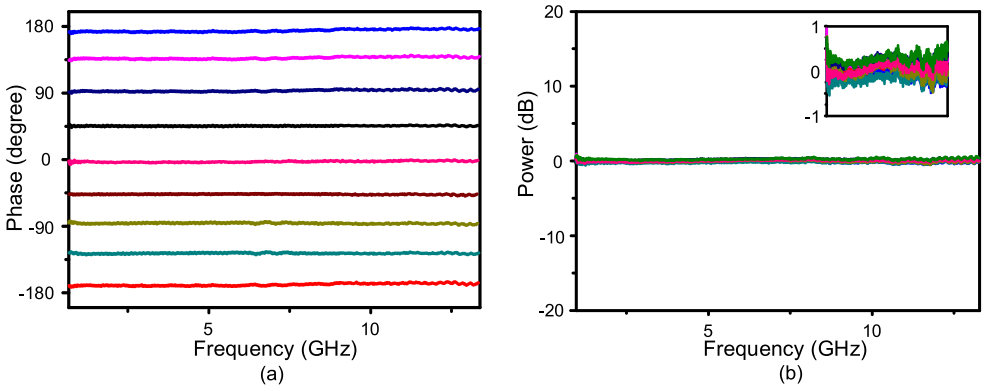

Fig. 3. (a) The phase response and (b) the magnitude response of the phase-shifted frequency-mixer.

PDM-DPMZM. An automatic bias controller is employed to control the dc biases of the modulator. The signal is then split into two paths via a 50:50 optical coupler, and each path followed by a polarization controller (PC), a polarization beam splitter (PBS) and a PD. The PC together with the PBS performs as a polarizer. The PD has a bandwidth of 30 GHz and a responsivity of 0.65 A/W, which is used to perform optical-to-electrical conversion. The output signals of the two PDs are combined by a low-frequency electrical 90° hybrid (0.5–10 GHz).

Fig. 2(a) displays the output optical spectra of the PDM-DPMZM when the frequencies of the LO and RF signals are 10 GHz and 12 GHz, which is observed with an optical spectrum analyzer (OSA, AQ6370C). As can be seen from Fig. 2(a), CS-SSB modulations are realized, and the optical carrier is more than 25–dB lower than the remained 1st-order sidebands. To confirm that the two peak sidebands are orthogonally polarized, a PBS is connected, and the two outputs of the PBS are shown as the black dashed line (12 GHz) and red dotted line (10 GHz) in Fig. 2(b). As can be seen, the two sidebands are well separated in two orthogonal polarization directions, and the polarization extinction ratio is $\sim$20 dB.

The orthogonally-polarized wavelengths are then split into two paths to realize a two-channel phase shifter. The frequency response of one channel of the phase shifter is measured with the LO signal fixed at 10 GHz and the RF signal sweep from 10.2 to 23 GHz. Fig. 3(a) and (b) show the measured phase curves and magnitude responses of the phase shifter over 0.2 to 13 GHz when the polarizer is tuned. The VNA is adopted to measure the phase and magnitude responses. From the two figures we can see that the phases can be continuously tuned from -180 to 180 degree while the magnitudes keep almost unchanged. The maximum power variations of the magnitude

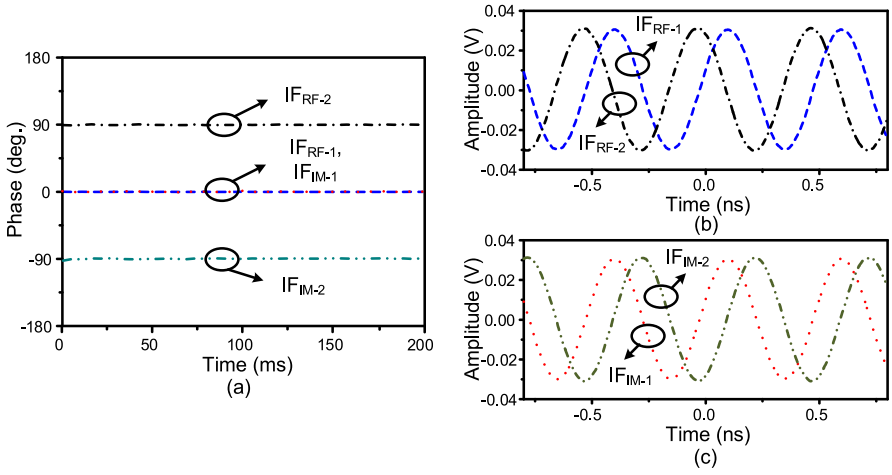

Fig. 4. The phases and waveforms of the IF signals at the outputs of PD1 and PD2. (a) The measured phases of the four generated IF signals, (b) the measured waveforms of the two RF-induced IF signals, and (c) the measured waveforms of the two image-induced IF signals.

response during the phase shifting is smaller than 1 dB, as shown in the zoom-in figure of Fig. 3(b), indicating that the phase shifter has a very flat power response.

Since the phases of the two channels of the phase shifter can be independently tuned by the polarizer in each channel, the quadrature phase conditions for image rejection can be easily satisfied. Taking a 10-GHz LO signal and a 12-GHz RF signal as an example, the phases and waveforms of the generated 2-GHz IF signals from the two channels of the phase-shifter are measured. The waveform is observed by a digital sampling oscilloscope (Agilent 86100C). As can be seen from the blue dashed and black dash-dotted curves in Fig. 4(a) and (b), the phase of the RF-induced IF signal from PD1 ($IF_{RF\text{-}1}$) is 90 degree lagged behind the RF-induced IF signal from PD2 ($IF_{RF\text{-}2}$). Then, the frequency of the RF signal is adjusted to be 8 GHz (the image frequency), and the phases and waveforms of the image-induced IF signals are shown in Fig. 4(a) and (c). From the red dotted and green dash-dot-dotted curves in Fig. 4(a) and (c) we can obtain that the image-induced IF signal from PD1 ($IF_{IM\text{-}1}$) is 90 degree advanced of the image-induced IF signal from PD2 ($IF_{IM\text{-}2}$).

With an electrical 90 degree hybrid to combine the outputs of the two PDs, the phases of the IF signals at the output of the hybrid changed. As can be seen from Fig. 5(a), the phases of the two RF-induced IF signals are the same while that of the two image-induced IF signals are complementary. Fig. 5(b) and (c) show the waveforms of the RF-induced and image-induced IF signals after the 90 degree hybrid, respectively, where the amplitude of the RF-induced IF signal is twice of the signal before the 90 degree hybrid while that of the image-induced IF signal is almost 0. The electrical spectra of the RF-induced IF signal and the image-induced IF signal are illustrated in Fig. 6. As can be seen, the image suppression ratio is about 60 dB.

To evaluate the broadband operation capability of the proposed IRM, linearly frequency-modulated (LFM) signals with bandwidths of 1 GHz (11–12 GHz), 2 GHz (11–13 GHz) and 4 GHz (12–16 GHz) are served as the RF signals, and the LO signal is fixed at 10 GHz. The LFM signal is then down-converted by the proposed mixer to be 1–2 GHz, 1–3 GHz and 2–6 GHz, as the black solid curves of Figs. 7(a), (b) and (c) show. Then the frequency range of the LFM signals are changed to be the image frequencies (8–9 GHz, 7–9 GHz and 4–8 GHz), and the output spectra of the IF signals are shown as the red dotted curves of Fig. 7. As can be seen, the image rejection ratios for 1-GHz, 2-GHz and 4-GHz bandwidths are about 35, 28 and 23 dB, respectively. The relatively smaller image rejection ratios for the larger bandwidth conditions is mainly due to the smaller power spectral density of the driving LFM signals and the power variations over the large frequency range.

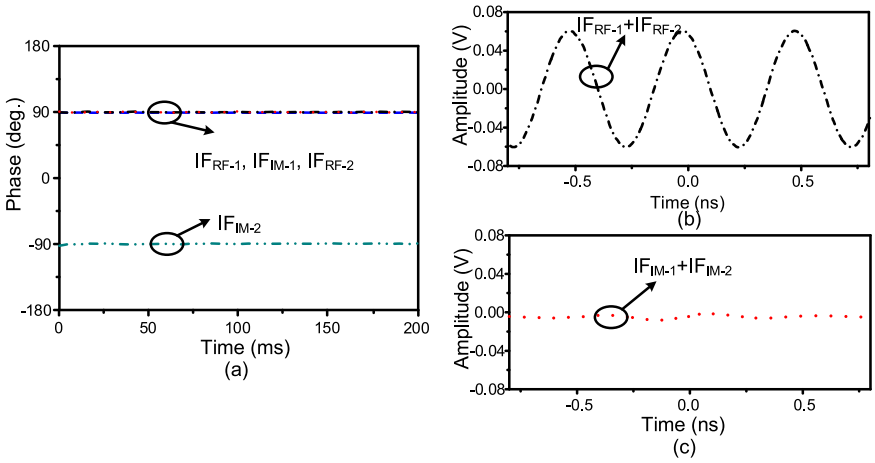

Fig. 5. The phases and waveforms of the IF signals at the outputs of the 90 degree hybrid. (a) The measured phases of the four generated IF signals, (b) the measured waveform of the RF-induced IF signal, and (c) the measured waveform of the image-induced IF signal.

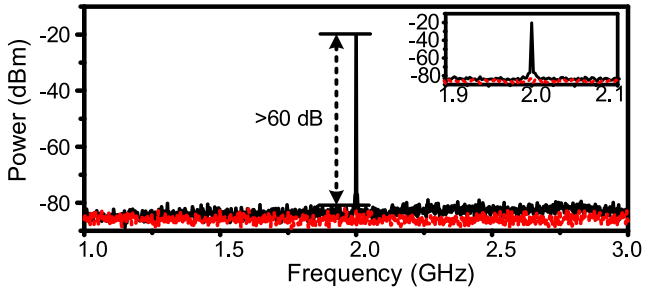

Fig. 6. The electrical spectra of the RF-induced IF signal (black solid curve) and the image-induced IF signal (red dotted curve).

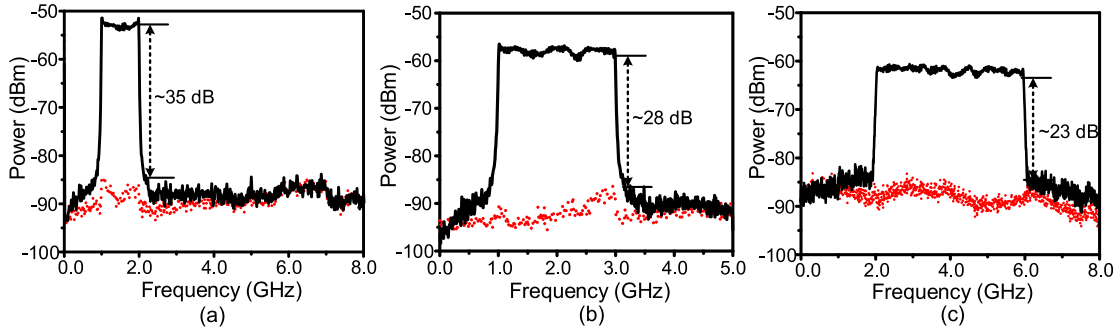

Fig. 7. The electrical spectra of the IF-LFM signals introduced by the LFM signal (black solid curve) and the image signal (red dotted curve), (a) 1-GHz bandwidth, (b) 2-GHz bandwidth, and (c) 4-GHz bandwidth.

The dynamic range of the proposed mixer is also measured when only one channel is enabled. A two-tone signal with frequencies of 12 GHz and 12.02 GHz is employed as the RF signal. The frequency and the power of the LO signal are fixed at 10 GHz and 10 dBm. When the power of the two-tone RF signal is swept from −25 to 25 dBm, the power of the fundamental term and the third-order intermodulation distortions (IMD3) are recorded and displayed in Fig. 8. Supposing the

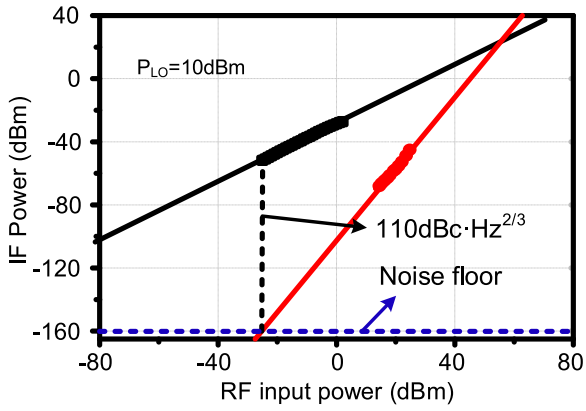

Fig. 8. Measured powers of the fundamental and IMD3 components as a function of the RF input power, the power of the LO signal is fixed at 10 dBm.

TABLE 1
Performance Comparison With Difference IRMs

Ref.	Method	IRR/single-frequency signal [dB]	IRR/Broadband signal [dB]	SFDR [dB·Hz$^{2/3}$]
[12]	Electrical filtering	150	NA	106
[14]	Optical filtering	20	NA	107
[22]	Hartley	57.2	NA	108
[23]	Hartley	60	35/50MHz	NA
Our work	Hartley	60	~23/4GHz	110

IRR: image rejection ratio; SFDR: Spurious free dynamic range.

noise floor is at −160 dBm/Hz (a general noise floor of a laser source), the spurious free dynamic range (SFDR) of the phase-shifted mixer is calculated to be about 110 dBc·Hz$^{2/3}$.

4. Conclusion

In conclusion, a novel IRM based on a two-channel polarization-modulated photonic microwave phase shifter was proposed and experimentally demonstrated. The two-channels of the polarization-modulated phase shifter can be independently and continuously tuned from −180 degree to 180 degree over 0.2 to 13 GHz (with LO fixed at 10 GHz) by adjusting the polarizer in each channel, so the quadrature phase conditions for image rejection can be easily satisfied. An IRM was realized. The image rejection performance of the IRM was evaluated, an image rejection ratio of ∼60 dB for single frequency signals was obtained. The broadband operation was also investigated. Image rejection ratios of 35 dB for 11–12 GHz LFM signal, 28 dB for 11–13 GHz LFM signal, and 23 dB for 12–16 GHz LFM signal (with LO fixed at 10 GHz) were achieved. Compared with other IRMs, the proposed IRM shows a good performance for broad instantaneous bandwidth image suppression, as can be seen from Table 1. The SFDR of the IRM under an assumptive noise floor of −160 dBm/Hz was ∼110 dBc·Hz$^{2/3}$. The proposed mixer can be potentially scaled to be a multi-channel mixer, which would find applications in broadband RF frontends and radio over fiber systems.

References

[1] J. Capmany and D. Novak, "Microwave photonics combines two worlds," *Nature Photon.*, vol. 1, no. 6, pp. 319–330, 2007.
[2] D. Zhu and S. L. Pan, "Photonics-based microwave image-reject mixer," *MDPI Photon.*, vol. 5, no. 2, p. 6, Mar. 2018.
[3] S. L. Pan *et al.*, "Satellite payloads pay off," *IEEE Microw. Mag.*, vol. 16, no. 8, pp. 61–73, Sep. 2015.
[4] J. Yao, "Microwave photonics," *J. Lightw. Technol.*, vol. 27, no. 3, pp. 314–335, Feb. 2009.
[5] P. Ghelfi *et al.*, "A fully photonics-based coherent radar system," *Nature*, vol. 507, no. 7492, pp. 341–345, 2014.
[6] D. Shan, A. J. Wen, W. Zhai, X. Li, W. Zhang, and Z. Tu, "Filter-free image-reject microwave photonic downconverter based on cascaded modulators," *Appl. Opt.*, vol. 58, no. 13, pp. 3432–3437, 2019.
[7] R. Zhu, B. Hraimel, and X. Zhang, "Analysis of simultaneous photonic frequency downconversion and optical subcarrier modulation in an electroabsorption modulator," *J. Lightw. Technol.*, vol. 30, no. 3, pp. 344–354, Feb. 2012.
[8] E. H. W. Chan and R. A. Minasian, "Microwave photonic downconverter with high conversion efficiency," *J. Lightw. Technol.*, vol. 30, no. 23, pp. 3580–3585, Dec. 2012.
[9] Y. S. Gao, A. J. Wen, W. Jiang, Y. Y. Fan, Y. He, and D. Y. Zhou, "Fundamental/subharmonic photonic microwave I/Q up-converter for signal sideband and vector signal generation," *IEEE Trans. Microw. Theory Technol.*, vol. 66, no. 9, pp. 4282–4292, Sep. 2018.
[10] C. J. Yin *et al.*, "Broadband lower-IF RF receiver based on microwave photonic mixer and Kramers-Kronig detection," *Opt. Express*, vol. 26, no. 20, pp. 26400–26410, 2018.
[11] A. C. Lindsay, G. A. Knight, and S. T. Winnall, "Photonic mixers for wide bandwidth RF receiver applications," *IEEE Trans. Microw. Theory Technol.*, vol. 43, no. 9, pp. 2311–2317, Sep. 1995.
[12] S. J. Strutz and K. J.Williams, "A 0.8-8.8-GHz image rejection microwave photonic downconverter," *IEEE Photon. Technol. Lett.*, vol. 12, no. 10, pp. 1376–1378, Oct. 2000.
[13] C. B. Albert, C. J. Huang, and E. H. W. Chan, "Brillouin-assisted notch filtering based all-optical image rejection mixer," *IEEE Photon. J.*, vol. 11, no. 2, Apr. 2019, Art. no. 7202712.
[14] S. J. Strutz and K. J. Williams, "An 8-18 GHz all-optical microwave downconverter with channelization," *IEEE Trans. Microw. Theory Technol.*, vol. 49, no. 10, pp. 1992–1995, Oct. 2001.
[15] X. Kong, Y. Yu, H. T. Tang, and X. L. Zhang, "Microwave photonic image-reject mixer based on a tunable microwave photonic filter with high rejection," *IEEE Photon. J.*, vol. 10, no. 6, Dec. 2018, Art. no. 5502411.
[16] D. Zhu, W. J. Chen, and S. L. Pan, "Photonics-enabled balanced hartley architecture for broadband image-reject microwave mixing," *Opt. Express*, vol. 26, no. 21, pp. 28022–28029, 2018.
[17] Z. Z. Tang, Y. F. Li, J. P. Yao, and S. L. Pan, "Photonics-based microwave frequency mixing: Methodology and applications," *Laser Photon. Rev.*, vol. 14, no. 1, 2020, Art. no. 1800350.
[18] Z. Y. Meng *et al.*, "Dual-band dechirping LFMCW radar receiver with high image rejection using microwave photonic I/Q mixer," *Opt. Express*, vol. 25, no. 18, pp. 22055–22065, 2017.
[19] Z. Shi, S. Zhu, M. Li, N. H. Zhu, and W. Li, "Reconfigurable microwave photonic mixer based on dual-polarization dual-parallel Mach-Zehnder modulator," *Opt. Commun.*, vol. 428, pp. 131–135, 2018.
[20] Z. Y. Tu, A. J. Wen, W. Zhang, Z. G. Xiu, and G. C. Yu, "All-optical image-reject frequency down-conversion based on cascaded electro-optical modulators," *Opt. Commun.*, vol. 430, pp. 158–162, 2019.
[21] J. Zhang J, E. H. W. Chan, X. D. Wang, X. H. Feng, and B. O. Guan, "High conversion efficiency photonic microwave mixer with image rejection capability," *IEEE Photon. J.*, vol. 8, no. 4, Aug. 2016, Art. no. 3900411.
[22] Y. S. Gao, A. J. Wen, W. Chen, and X. Li, "All-optical, ultra-wideband microwave I/Q mixer and image-reject frequency down-converter," *Opt. Lett.*, vol. 42, no. 6, pp. 1105–1108, 2017.
[23] Z. Z. Tang and S. L. Pan, "Image-reject mixer with large suppression of mixing spurs based on a photonic microwave phase shifter," *J. Lightw. Technol.*, vol. 34, no. 20, pp. 4729–4735, Oct. 2016.
[24] P. X. Li, W. Pan, X. H. Zou, B. Lu, L. S. Yan, and B. Luo, "Image-free microwave photonic down-conversion approach for fiber-optic antenna remoting," *IEEE J. Quantum Electron.*, vol. 53, no. 4, Aug. 2017, Art. no. 9100208.
[25] W. Zhang, A. J. Wen, Y. S. Gao, S. Shang, H. X. Zheng, and H. Y. He, "Large bandwidth photonic microwave image rejection mixer with high conversion efficiency," *IEEE Photon. J.*, vol. 9, no. 3, Jun. 2017, Art. no. 7201908.
[26] T. Lin, E. H. W. Chan, X. D. Wang, X. H. Feng, B. O. Guan, and J. P. Yao, "Broadband photonic microwave signal processor with frequency up/down conversion and phase shifting capability," *IEEE Photon. J.*, vol. 10, no. 1, Feb. 2018, Art. no. 5500112.
[27] Y. M. Zhang and S. L. Pan, "Broadband microwave signal processing enabled by polarization-based photonic microwave phase shifters," *IEEE J. Quantum Electron.*, vol. 54, no. 4, Aug. 2018, Art. no. 0700112.
[28] Y. M. Zhang and S. L. Pan, "Photonics-based multi-function analog signal processor based on a polarization division multiplexing Mach–Zehnder modulator," *Opt. Lett.*, vol. 42, no. 23, pp. 5034–5037, 2017.